LA-5949-MS

a. 3

UC-34c
Reporting Date: April 1975
Issued: June 1975

Neutron Spectrum from an Oralloy Sphere

by

Charles E. Ragan
George F. Auchampaugh
Arthur Hemmendinger
Myron G. Silbert

los alamos
scientific laboratory
of the University of California
LOS ALAMOS, NEW MEXICO 87544

UNITED STATES
ENERGY RESEARCH AND DEVELOPMENT ADMINISTRATION
CONTRACT W-7405-ENG. 36

Printed in the United States of America. Available from
National Technical Information Service
U S Department of Commerce
5285 Port Royal Road
Springfield, VA 22151
Price: Printed Copy $4.00 Microfiche $2 25

NEUTRON SPECTRUM FROM AN ORALLOY SPHERE

by

Charles E. Ragan, George F. Auchampaugh, Arthur Hemmendinger, and Myron G. Silbert

ABSTRACT

The neutron spectrum from a 38-kg oralloy sphere, pulsed by a centrally located 14-MeV neutron source, has been measured using time-of-flight (TOF) techniques. The nearly isotropic source of 14-MeV neutrons was produced by bombarding a tritium gas target with low-energy deuterons. Neutrons in the 0.180- to 15.0-MeV energy range were detected at the end of a partially evacuated, 39-m flight path by a NE-213 liquid scintillator that used pulse shape discrimination to distinguish neutron events from gamma-ray events. Detector thresholds of 0.15 and 0.85 MeV were used to cover the above energy range, and the detector efficiency was measured over this range using monoenergetic neutrons from the T(p,n), T(d,n), and D(d,n) reactions. Several measurements of the TOF spectrum were used to determine the neutron flux at the detector, and a comparison of this flux with the results of Monte Carlo calculations is presented. These calculations were performed with the code MCN using two cross-section sets, those from the Lawrence Livermore Laboratory (LLL) and those from the ENDF/B-IV library. The results calculated using the ENDF/B-IV cross sections are in excellent agreement with the measurements, especially in the 1- to 6-MeV energy region, where the uncertainties in both the calculated and experimental results are the smallest.

I. INTRODUCTION

The Los Alamos Scientific Laboratory's (LASL) Theoretical Design Division has requested measurements of fission densities as a function of position in various assemblies.[1] These measurements will be used as benchmarks in evaluating Monte Carlo calculations, and the conclusions should be widely applicable. Common to each assembly mentioned above is a hollow 38-kg oralloy (93.5% ^{235}U, 6.5% ^{238}U) sphere which will be the component directly surrounding an approximately isotropic source of 14-MeV neutrons. Knowledge of the neutron energy spectrum from this sphere is necessary to make accurate calculations of fission densities in the specified assemblies. Therefore, as a first step in this program, a measurement of this spectrum was undertaken, and a preliminary report[2] on this measurement was prepared for the Theoretical Design Division.

II. ACCELERATOR

Several accelerators capable of producing nearly isotropic pulses of 14-MeV neutrons exist at LASL. These accelerators are basically of two types: Cockcroft-Walton accelerators which produce 14-MeV neutrons from the T(d,n) reaction using 300- to 400-keV deuterons and Van de Graaff accelerators

capable of producing neutrons with a wide range of energies from various reactions. At a pulse rate of 2.5 MHz, one Cockcroft-Walton accelerator is capable of producing $\sim 5 \times 10^8$ neutrons/s using a solid tritium-zirconium target, whereas the Van de Graaff accelerators are capable of producing about 10^9 neutrons/s from the T(d,n) reaction at approximately this same pulse rate using a tritium gas target. From this standpoint, neither machine has an obvious advantage. High-resolution neutron time-of-flight (TOF) measurements require accurate timing (<1 ns) over a wide time interval. These requirements dictate the use of fast, sophisticated electronics for digitizing the data and the use of an on-line computer for data storage. Only the Van de Graaff accelerators in LASL's Group P-9 are equipped in this manner; therefore, they were chosen for the TOF measurements.

The two Van de Graaff accelerators at P-9 are a vertical, single-ended machine capable of providing 1- to 6-MeV deuterons and a tandem FN accelerator capable of providing 4- to 18-MeV deuterons. As the deuteron energy is increased above 110 keV, the yield from the T(d,n) reaction decreases substantially, the neutron energy spread increases, and the degree of isotropy decreases. Consequently, the deuterons from either P-9 machine must be reduced in energy before interacting with the tritium. This can be accomplished by using an entrance foil to the gas target of the appropriate thickness.

The deuterons from the vertical accelerator need to be degraded in energy only slightly, thereby requiring a much thinner foil with less energy straggling. This machine, however, has several unfavorable features. (1) The energy resolution obtainable in TOF depends upon the length of the flight path. When this experiment was being planned, the construction of a 40-m flight path was under way at the tandem, and there were no provisions for a flight path of this length on the vertical. (2) To detect low-energy neutrons, the time between pulses must be such that these neutrons can reach the detector before high-energy neutrons arrive from the next beam pulse. The pulse rate at the vertical machine is essentially fixed at 2.0 MHz, whereas the pulse rate on the tandem can be decreased in steps of two from 2.5 MHz to 78.125 kHz. Therefore the tandem accelerator was chosen for the spectrum measurements, with the accepted disadvantage of more straggling in the entrance foil to the gas cell.

At the higher beam energies necessary on the tandem, a larger background of neutrons was produced in the entrance foil. This background decreased substantially with decreasing energy, but so did the beam current. At a beam energy of 4 MeV, the available current was down by more than an order of magnitude from the maximum. Thus, the choice of the beam energy was a trade-off between beam current and background, with the exact energy determined by the entrance foil thickness.

After selecting the facility, it was necessary to complete the installation of the flight tube, install the target and tritium gas handling system, determine the characteristics of the neutron source, install a detector system at the end of the flight tube, and construct a support for the oralloy sphere. The details of this work are described in the following sections.

III. NEUTRON SOURCE

For a thin target, the peak cross section[3-5] for the T(d,n) reaction occurs at approximately 110 keV. At this energy, the angular distribution of neutrons can be calculated from the reaction kinematics, assuming an isotropic distribution in the center of mass. However, when a thick entrance window and target are used, the angular distribution needs to be determined experimentally.

Measurements of the source characteristics were performed on the R-2 beam leg of the tandem accelerator. Figure 1 shows the experimental setup. The detector system was the same as used for the spectrum measurements, with the low-energy threshold set at approximately 0.85 MeV. The detector and shield were placed on a cart that rotated about the center of the gas cell (Fig. 2). The pressure seal for the gas cell consisted of two indium gaskets and a molybdenum foil. The cell was filled through the 1.1-mm-diam hypodermic tubing and was insulated from the beam tube and from the gas handling apparatus to allow current integration.

Measurements were made at a tritium pressure of 0.204 MPa gauge (30 psig) using molybdenum entrance foils of two thicknesses—50 and 63.5 μm. These thicknesses correspond to the range of 4.6- and 5.3-MeV deuterons in molybdenum, respectively. Figure 3 shows the measured neutron yield from the T(d,n) reaction as a function of bombarding energy at 90° to the beam for these two foils. The peak in the yield is caused by the 110-keV resonance in the T(d,n) cross section. At beam energies below the peak, the transmitted deuterons are below the resonance, and at beam energies above the peak, the deuterons do not lose sufficient energy in the tritium to reach the resonance from above. Most of the neutrons at the peak of the yield are therefore produced by 100 to 200-keV deuterons, and

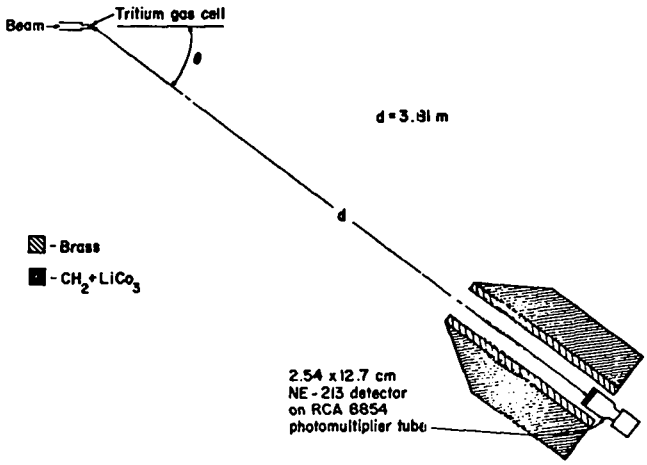

Fig. 1.
Experimental setup used for determining the energy and yield as a function of angle (θ) for the 14-MeV neutron source. The neutrons were detected with a shielded NE-213 detector mounted on an RCA-8854 photomultiplier tube placed 3.81 m from the source. The angle θ varied from 0 to 135°.

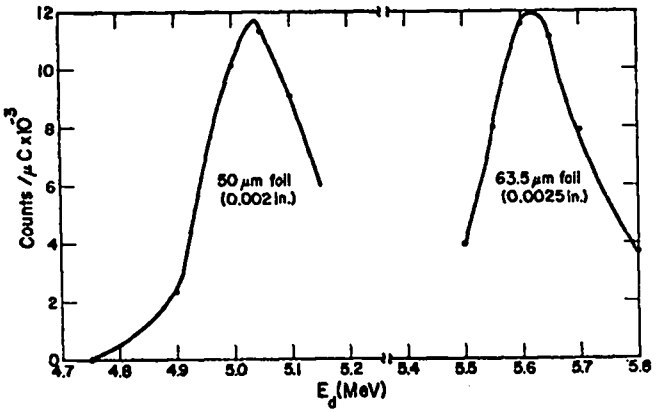

Fig. 3.
Plots of the counts per microcoulomb in the 14-MeV neutron peak for the 50-μm foil and for the 63.5-μm foil as a function of deuteron energy. The solid line is drawn to guide the eye. The yield is about the same for the two foils and the peak yields occur at about 5.05 and 5.60 MeV for the 50- and 63.5-μm foils, respectively.

calculations indicate that the average deuteron energy is approximately 150 keV.

Typical TOF spectra recorded at 0 and 90° to the beam are shown in Fig. 4, and the T(d,n) neutrons are seen to be well separated from the background. The yield from the T(d,n) reaction varied only slightly with angle. However, the yield of the background neutrons was extremely forward peaked. The angular distributions of the neutrons in the background at incident beam energies of 5.05 and 5.6 MeV, corresponding to the peak yields, are shown in Fig. 5. These yields are plotted in counts per microcoulomb without correction for the detector efficiency to indicate the manner in which the yield changes with angle. The integrated background at

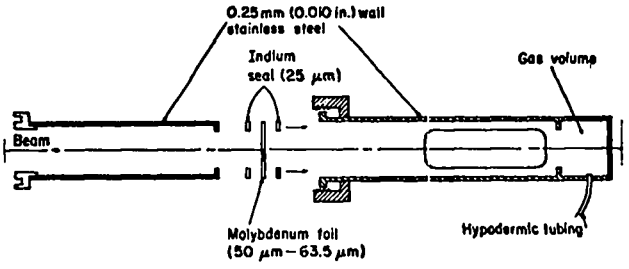

Fig. 2.
Exploded view of the tritium gas target assembly used as a source of 14-MeV neutrons from the T(d,n) reaction. The deuteron beam enters from the left and passes through the molybdenum foil before entering the gas. The foil is sealed between the two sets of flanges by the indium gaskets.

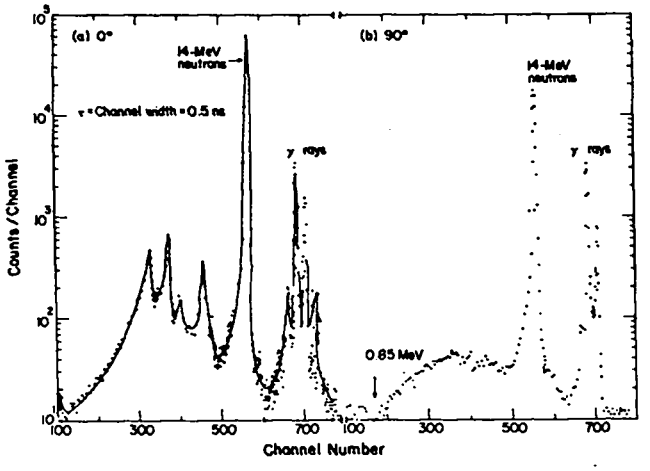

Fig. 4.
Sample spectra obtained using the experimental setup shown in Fig. 1 at a bombarding energy of 5.05 MeV with a 50-μm-thick foil. Both spectra were recorded using 0.5-ns channel widths. Spectrum (a) was recorded with the detector at 0° to the beam and the background is much larger than in (b), which was recorded with the detector at 90°.

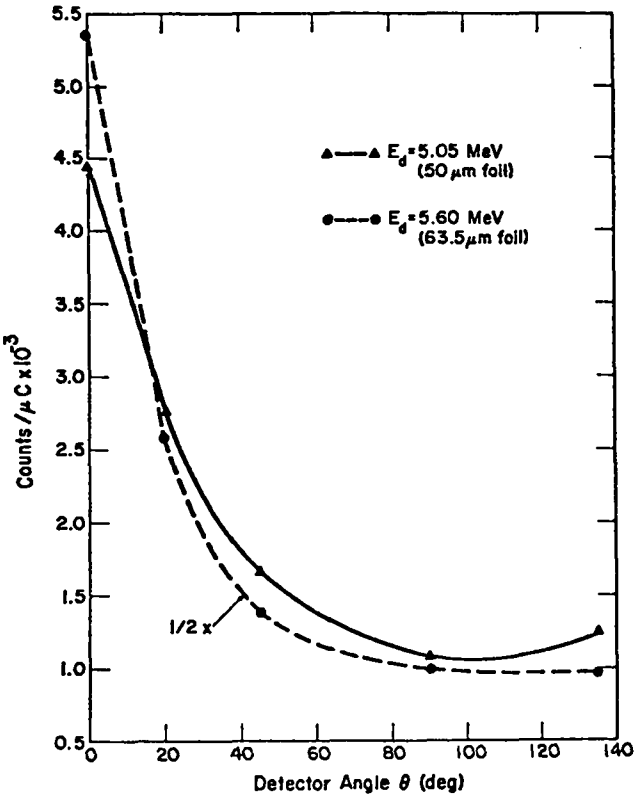

Fig. 5.
Plots in counts per microcoulomb of the angular distribution of background neutrons obtained with two foil thicknesses and beam energies. The data obtained at a deuteron energy of 5.60 MeV (63.5-μm foil, ●) are about a factor of two higher than the data obtained at a beam energy of 5.05 MeV (50 μm foil, ▲).

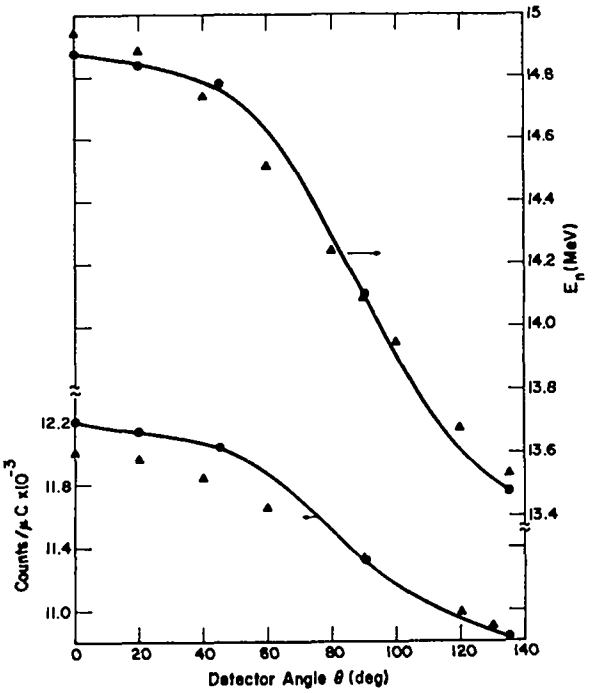

Fig. 6.
Plots of the variation of energy (upper) and yield (lower) with angle for 14-MeV neutrons from the T(d,n) reaction at an effective deuteron energy of ~150 keV. These neutrons were produced by 5.05-MeV deuterons incident on a gas cell with a 50-μm-thick molybdenum entrance foil. The ▲'s represent the values calculated from the reaction kinematics (see text) and are in good agreement with the measured (●) values. The lines are drawn to guide the eye.

5.6 MeV is larger than that at 5.05 MeV by approximately a factor of two. Thus, a 50-μm entrance window and a 5.05-MeV beam energy were chosen for the spectrum measurements. At this beam energy the integrated background yield is 6% of the integrated yield of neutrons from the T(d,n) reaction.

Figure 6 shows plots of the measured (●) and calculated (▲) energy and yield as a function of angle for neutrons from the T(d,n) reaction at a deuteron energy of 5.05 MeV, corresponding to the peak of the yield curve for the 50-μm molybdenum foil. The energy and yield were calculated from the reaction kinematics for a deuteron energy of 150 keV, and for the yield calculations an isotropic distribution in the center of mass was assumed. These calculated results represent the measured values quite accurately. The yield appears to be antisymmetric about 90° and changes by only 7.7% in going from 90 to 0°.

For the actual spectrum measurements from the oralloy sphere, a tritium gas cell was mounted on an insulated snout at the end of the 0° beam tube of the tandem accelerator. The hypodermic filling tube was connected through a ceramic insulator to a uranium furnace containing approximately 100 cm^3 of tritium trapped in the uranium. This furnace was heated to release the tritium into the gas cell. Also connected to the hypodermic tubing was a piezoresistive transducer with digital readout for

measuring gas pressure. The pressure could be reproduced to 1% using this device, and variations of 0.1% during a run could be noted.

IV. MULTIPLYING ASSEMBLY

The hollow oralloy sphere designated MA-0 is detailed in LASL drawings 32Y-20935-C4, 5, and 8, and is shown schematically in Fig. 7. The sphere is parted along a diametrical plane, and in this plane there are three holes which accommodate parts of the target for the Cockcroft-Walton accelerator. Each half of the sphere is composed of three hemispherical shells which fit together to form a hollow sphere with an inner radius of 2.225 cm, an outer radius of 7.799 cm, and a mass of 37.764 kg.

For the spectrum measurements, the hemispheres were positioned with the largest radial hole around the insulated snout and with the gas cell in the center of the spherical cavity. The hypodermic filling tube passed through the radial hole in the sphere at right angles to the largest one. Electrical tape was used to ensure that the sphere did not touch any portion of the target, which would have shorted out the current integrating system. A pneumatic lift mechanism detailed in LASL drawing 70Y-157044-D1-5 and shown in Fig. 8 was used to support and assemble the two hemispheres. Also shown in Fig. 8 are the two cadmium-clad hemispheres positioned around the tritium target with the lift mechanism in the down position.

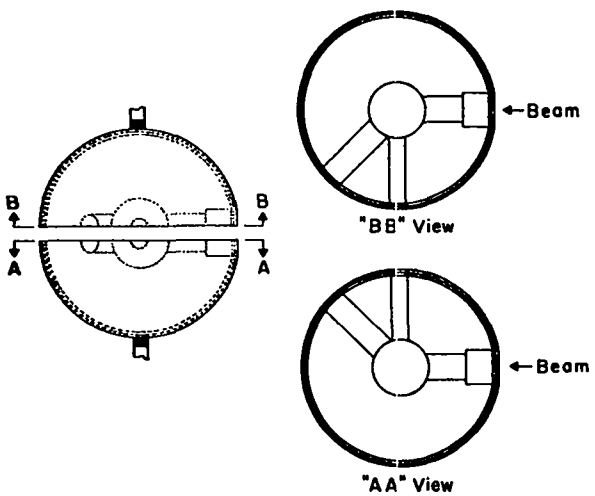

Fig. 7.
Schematic of the 37.764-kg oralloy sphere. The sphere is parted along a diametrical plane and the three holes in this plane are to accommodate parts of the target for the Cockcroft-Walton accelerator.

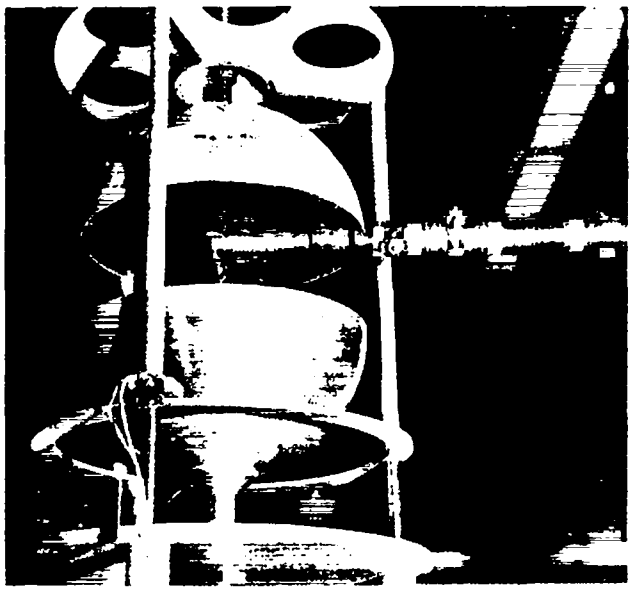

Fig. 8.
Photograph showing the oralloy sphere and the pneumatic lift mechanism. The top hemisphere is suspended in place, and the bottom hemisphere is lowered to show the tritium gas cell in the central cavity.

V. NEUTRON DETECTOR AND ELECTRONICS

Neutrons were detected with a 2.54-cm-thick by 12.70-cm-diam NE-213 liquid scintillator mounted on an RCA-8854 photomultiplier tube. A schematic of the detailed electronics is shown in Fig. 9. The fast output (anode) from the tube base was shaped by a constant fraction discriminator to provide start signals from the detector. Stop signals were provided by a delayed pulse obtained from a capacitative beam pickoff. Each start-stop pair was converted to digital time information using a 62.5-MHz EG&G clock with a timing resolution of 0.125 ns. This time information was stored in the SDS-930 on-line computer with 8-ns channel widths. By using the different rise-time characteristics of the NE-213 scintillator for neutrons and gamma rays,[6] a tag pulse was generated for each detector pulse. These tags were used to route the neutron and gamma-ray TOF spectra to different portions of memory in the computer. At the end of each run the spectra in the computer were written onto magnetic tape for later analysis using the CDC-6600 computer.

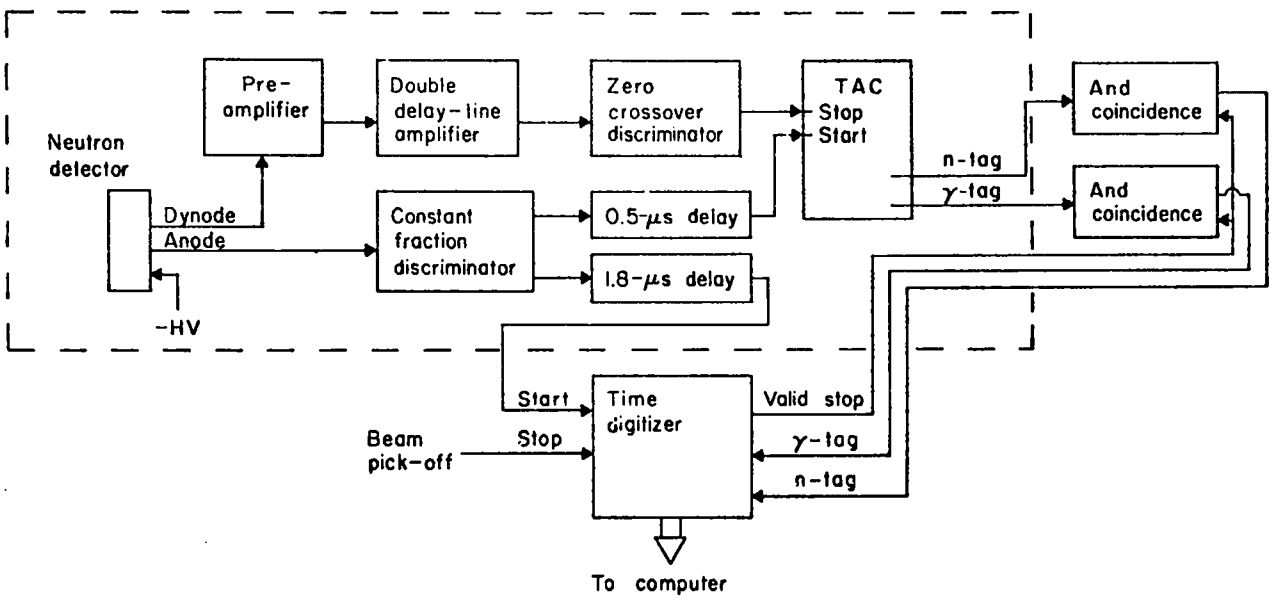

Fig. 9.
Electronics setup used in the measurement of the spectrum from the oralloy sphere. The anode output was used to provide a fast timing pulse, and the dynode output was used with the anode output to form a tag signal to identify the anode signal as a neutron or gamma ray. This distinguishing signal came from the time-to-amplitude converter (TAC) and originated because the NE-213 scintillator has different rise times for neutrons (slow) and gamma rays (fast). The electronics within the dashed line were positioned near the detector and the remainder were near the computer.

To unfold the spectrum shape from the measured number of counts, it is necessary to know the efficiency of the detector as a function of energy. The shape of this curve without n,γ discrimination can be calculated because it depends on the neutron-proton cross section, the detector thickness, and the detector bias or low-energy threshold. However, the effectiveness of the n,γ discrimination is a function of energy; therefore the efficiency must be determined experimentally.

Saturation effects in the n,γ discrimination circuit cause some high-energy neutrons to be tagged as gamma rays, thereby limiting the dynamic range of the system. The pulse height output of NE-213 is not linear in neutron energy,[7] and the energy range from 0.2 to 17 MeV represents a dynamic range of approximately 600. Therefore, this energy range was covered in two steps by using two different high voltages on the photomultiplier tube. A bias of −2100 V was used to cover the range from approximately 1.4 to 17.0 MeV and a bias of −2600 V was used for the range <0.2 to ~5.0 MeV. The relative detector efficiency was measured at both voltages over the above energy ranges.

This efficiency was measured using monoenergetic neutrons produced by charged particle reactions with known[8,9] cross sections. The tandem accelerator provided monoenergetic neutrons with energies ≥3.5 MeV at 0° from the T(p,n), T(d,n), and D(d,n) reactions. The efficiency measurements at these neutron energies involved only determining the relative number of counts in the neutron peak and normalizing to the cross section and to the integrated beam current after correcting for dead time (<5%). In these measurements the beam straggling in the 10.6-mg/cm^2 molybdenum entrance window to the gas target was small. For neutron energies below 6.0 MeV, the efficiency was measured using the vertical accelerator. The two sets of measurements were normalized in the overlap region from 3.5 to 6.0 MeV. In the 1- to 6-MeV energy range, the T(p,n) reaction at 0° was used as a monoenergetic neutron source. Neutrons below 1 MeV were obtained from the T(p,n) reaction at angles other than 0°. The detector efficiency was extracted from these measurements by normalizing the counts in the neutron peak to the integrated current and to the T(p,n) cross section at the appropriate angle. In the measurements at low incident energy there was a considerable spread in the neutron energy due both to straggling in the molybdenum entrance foil and tritium gas, and to

kinematic broadening. These effects introduced uncertainties in the efficiency measurements, and they were amplified by the rapidly changing detector efficiency near threshold, where small changes in the energy or drifts in the electronics introduce large errors in efficiency.

Figure 10 shows plots of the relative efficiency curves at the two photomultiplier high voltages used in the spectra measurements. The efficiency near threshold showed small drifts during the time required to complete the spectra measurements (several months). For this and the above-mentioned reasons, larger errors have been assigned to these low-energy points. (See Sec. VIII.)

VI. FLIGHT TUBE

The flight path for measuring the spectrum using TOF techniques is 38.87 m from the center of the gas cell to the center of the detector. An evacuated 30.5-cm-diam iron pipe covers approximately 29 m, whereas air fills the remaining distance. The windows for the pipe consist of 125-μm Kapton ($C_{16}H_6O_4N_2$, $\rho = 1.42$ gcm^{-3}); Figure 11 is a photograph of one end of the iron pipe showing the window.

Two 1.2-m-long collimators were installed in the pipe. These collimators consist of 2.5-cm-wall iron pipes, with 15.24- and 16.51-cm inside diameters. The smaller collimator, located approximately 7.3 m

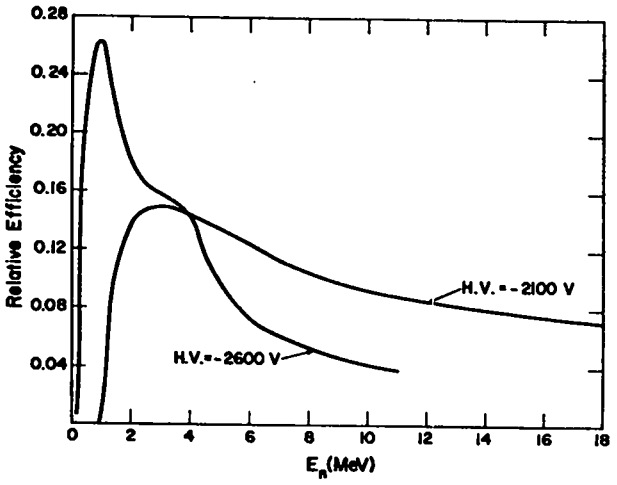

Fig. 10.
Plots showing the relative efficiency of the detector as a function of neutron energy. These efficiencies were measured at photomultiplier voltages of −2100 and −2600 V and correspond to thresholds of 0.85 and 0.15 MeV, respectively.

Fig. 11.
Photograph showing the end of the evacuated flight pipe nearer the detector with a stretched 125-μm Kapton window. The vacuum in the pipe was maintained at less than 60 x 10^{-3} torr.

from the source, defined the viewing area for the 12.70-cm-diam detector. Each collimator was located where the flight tube passes through a 0.9-m-thick concrete wall. The hole in the wall around the pipe was filled with lead, iron, and polyethylene shielding material. A schematic of the flight path is shown in Fig. 12. The entire pipe was aligned to better than 3 mm using a laser, and the collimators were positioned to an accuracy of 1 mm.

At the end of the flight tube, the detector and associated electronics were housed in a portable building (Fig. 13). The beam enters the building through a 125-μm-thick clear-polystyrene window. A traveling telescope mounted about 2 m behind the detector was used to locate the center of the beam. With the detector centered within 1 mm of the beam center, the collimating system allowed the detector to view a circular source with a diameter only 3 mm greater than that of the oralloy sphere.

VII. EXPERIMENTAL PROCEDURE

Three separate sets of measurements of the neutron spectrum from the oralloy sphere were performed on May 7, June 11, and August 29, 1974. For each set of measurements the two oralloy

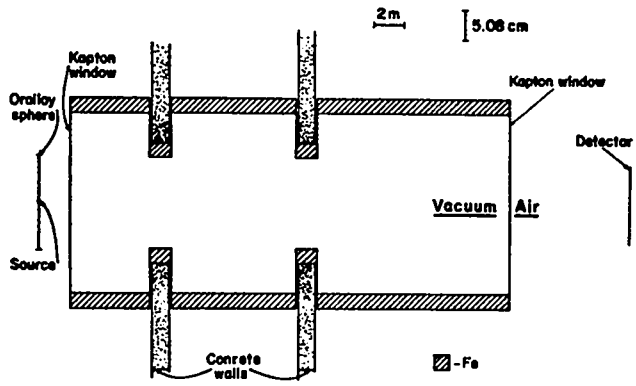

Fig. 12.
Flight path from the source to the detector showing the collimating system for limiting the detector field of view. Notice the scale differences in the two directions.

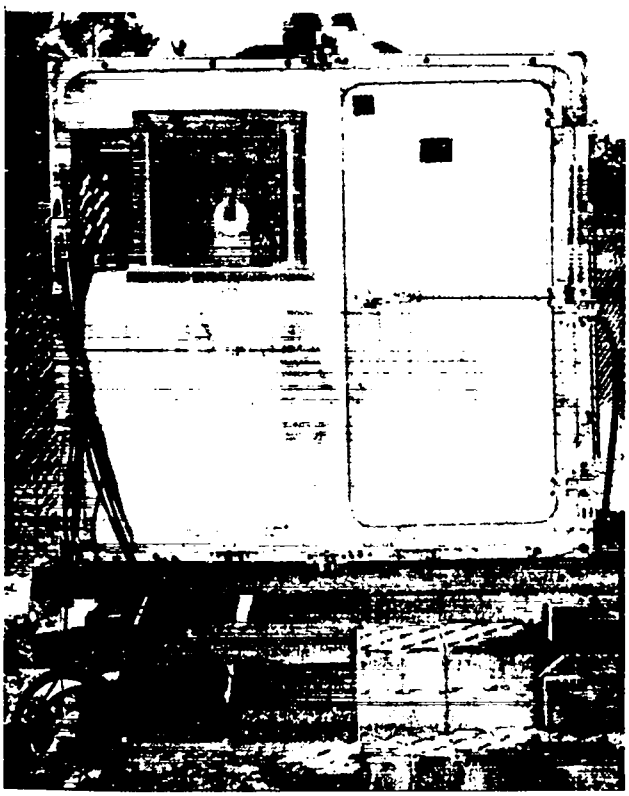

Fig. 13.
Portable building containing the detector (in the window) and the electronics within the dashed line of Fig. 9. Also shown at the left are the signal cables from the detector to the computer area.

hemispheres were transported in separate containers from the vault at LASL Group A-2 to LASL Group P-9. Each hemisphere was removed from its container, in the presence of an H-Division monitor, and was fitted inside a 0.76-mm-thick cadmium hemishell, which was used as a shield from thermal room-return neutrons.

Before beginning each series of runs, the low-energy threshold and n,γ discrimination properties of the detector were checked using ^{137}Cs and Pu(Be) sources, respectively. The target cell was filled with helium to check for pressure stability while the beam was being tuned on target. After making these checks, the gas cell was filled to 0.218 MPa gauge (32 psig) of tritium by heating the uranium furnace, and a spectrum of the bare source was recorded for a specified integrated current of incident deuterons. This run was also used to assure that the electronics were working properly.

The sphere was then positioned around the target using the assembly shown previously. As a precaution, when the two hemispheres were being assembled, the gamma-ray activity was monitored by detectors with an audible alarm. The parting plane of the sphere was tipped about 1° from horizontal so that it was not in line with the detector. In the May 7 runs, the sphere was not tilted and a 0.5-mm separation between the two hemispheres was responsible for an anomalously large number of source neutrons reaching the detector. However, the other portion of the spectrum was not affected by the separation. In the other runs, the separation between the hemispheres was less than 0.05 mm.

For each set of runs, several spectra were recorded with and without the oralloy sphere surrounding the tritium-filled gas cell. These runs provided a measurement of the transmission of 14-MeV neutrons, as well as a measure of the shape of the spectrum from the sphere. The gas cell was then evacuated and filled with helium gas to a pressure of 0.218 MPa gauge, and the time-of-flight measurements were repeated with and without the sphere. These spectra were used to measure the neutrons associated with the Mo(d,n) and other background reactions. For the May 7 and August 29 measurements, spectra were recorded with detector thresholds of approximately 0.15 and 0.85 MeV. For the June 11 measurements, spectra were recorded using only the 0.85-MeV threshold; however, five pairs of sphere-on and sphere-off runs were recorded to obtain an accurate measure of the transmission for 14-MeV neutrons. These five pairs of runs repeated within statistics, indicating accurate current integration and reproducibility in positioning the sphere.

The spectrum data were obtained at three different beam pulse rates. All of the data recorded with a detector threshold of approximately 0.15 MeV were obtained at a pulse rate of 78.125 kHz, with beam currents of 40 to 50 nA. Most of the data recorded with a detector threshold of about 0.85 MeV were obtained at a pulse rate of 0.3125 MHz and with beam currents of 180 to 200 nA, but some runs with this threshold were obtained at the lower pulse rate. The data used to determine the transmission of 14-MeV neutrons were obtained at a pulse rate of 1.25 MHz with beam currents of 0.5 to 0.6 μA. These pulse rates allowed the neutrons in the energy region of interest to reach the detector before the next beam pulse.

VIII. DATA REDUCTION AND RESULTS

Figure 14 shows typical spectra recorded with the sphere in place and with the cell filled with tritium and helium. These raw data in counts per channel were reduced to neutrons/MeV-cm^2 per source 14-MeV neutron to facilitate comparison with Monte Carlo calculations and to remove errors associated

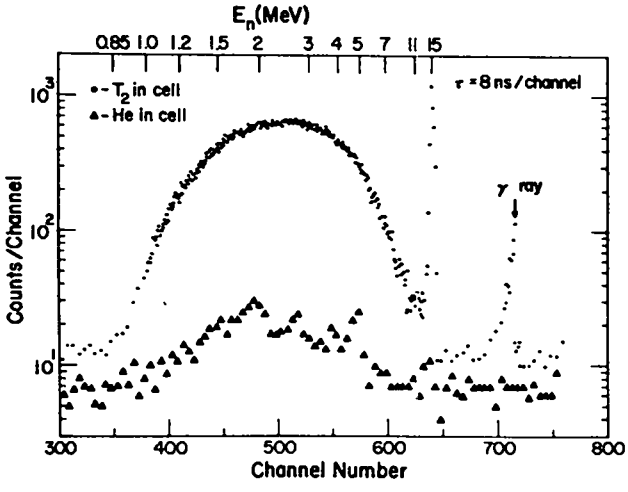

Fig. 14.
Plots of the raw data in counts per channel as a function of channel obtained with the sphere in place and with tritium (•) and helium (▲) in the cell. These spectra were recorded with a detector threshold of 0.85 MeV with channel widths of 8 ns. The integrated current for each spectrum was 10^5 μC, but the helium run used a slightly larger beam current and thus a shorter time. For this reason, the time-independent background is less than in the tritium run. The neutron energy in MeV is given along the top of the graph.

with uncertainties in the absolute detector efficiency. This reduction was accomplished in the following manner. If $N_i(E)dE$ is the number of neutrons detected with energy E in the interval dE by a detector of area A at the end of a flight path of length ℓ during the i^{th} run for C_i μC, then the number of source neutrons from an isotropic source per microcoulomb in the energy interval dE is given by

$$n_i(E)dE = \frac{4\pi\ell^2 N_i(E)dE}{A\, C_i \epsilon_b(E)} ,$$

where $\epsilon_b(E)$ is the detector efficiency for a threshold b. Thus the number of 14-MeV source neutrons per MeV from a bare isotropic source is given by

$$n_i(E) = \frac{4\pi\ell^2}{A\, C_i} \frac{1}{\bar{\epsilon}_b(14)} \sum_{14's} N_i(E) ,$$

where the sum is over the neutrons in the 14-MeV peak and where the average efficiency for 14-MeV neutrons $\bar{\epsilon}_b(14)$ has been removed from the summation. For an anisotropic source which is antisymmetric about 90° with $\alpha(\theta)$ representing the ratio of the number of neutrons per steradian at an angle θ to the average number emitted per steradian, the number of source 14-MeV neutrons is

$$n_i(E) = \frac{4\pi\ell^2}{A\, C_i\, \alpha(\theta)} \frac{1}{\bar{\epsilon}_b(14)} \sum_{14's} N_i(E) .$$

For the present source and detector, $\theta = 0°$ and $\alpha(0°) = 1.07$. Then for a run with the oralloy sphere in place, the number of neutrons at the detector per MeV-cm^2 per source 14-MeV neutron is

$$n_j(E) = \frac{N_j(E)/[\epsilon_b(E) C_j A]}{4\pi\ell^2 \sum_{14's} N_i(E)/[A\, C_i \alpha(0°) \bar{\epsilon}_b(14)]}$$

$$= \frac{N_j(E)\alpha(0°)}{\frac{C_j}{C_i} 4\pi\ell^2 \sum_{14's} N_i(E) \frac{\epsilon_b(E)}{\bar{\epsilon}_b(14)}}$$

where $N_j(E)$ is the number of detected neutrons per MeV for C_j μC. This number is obtained from $N_j(k)$, the net counts per channel in channel k, using the relation

$$N_j(E) = \frac{dk}{dE} N_j(k) = \frac{1}{\tau}\frac{t}{2E} N_j(k) \quad ,$$

where t is the flight time for neutrons of energy E and τ is the time per channel. The flight time and relativistically correct energy are calculated using the relations

$$t = \tau\left(|k-k_\gamma| + A\right) ,$$

and

$$E = 939.505\left[\left\{1 - \left[A/\left(A + |k-k_\gamma|\right)\right]^2\right\}^{-1/2} - 1\right] \quad ,$$

where the gamma-ray flight time is $A = 3.3356\ //\tau$ and k_γ is the gamma-ray channel.

The number of source neutrons

$$\sum_{14\text{'s}} N_i(E)$$

was obtained from the runs taken with the sphere removed and with tritium in the cell by summing the counts above a background obtained from a linear interpolation under the peak.

For the j^{th} run with the sphere in place, the net number of counts in the k^{th} channel $N_j(k)$ was obtained from the raw data in the following manner. First, the raw data were corrected for "dead time" by multiplying the counts in each channel by the ratio of the total number of start pulses to the number of start-stop pairs accepted by the computer. Then, two types of background were subtracted from the spectrum. A time-independent background not associated with the beam pulse was obtained for each channel by averaging many channels in the flat portion of the spectrum preceding the gamma-ray bursts. This background was obtained to an accuracy of a few percent and was less than 5% of the counts per channel in most cases. A time-dependent background was obtained from the runs with helium in the cell and with the sphere in place. These spectra were corrected for dead time and time-independent background, normalized to the integrated current, and subtracted channel by channel from the runs with tritium in the cell. This background was 1 to 5% of the total number of counts per channel.

Sample listings of the raw data obtained on August 29, 1974, using a detector threshold of 0.85 MeV with tritium or helium in the cell are given in Tables I and II, respectively. Table III lists the results obtained from these data for every fifth channel. The channel number and energy are given in columns 1 and 2. Column 3 gives the net spectrum after dead time corrections, and column 4 lists efficiency-corrected values for the neutrons/MeV-cm^2/source neutron at the detector. The statistical error associated with each channel is given in column 5.

These data were then averaged over the energy bins in Table IV for comparison with Monte Carlo calculations. This averaging was performed by finding the net number of neutrons per square centimeter for each energy bin and then dividing this sum by the energy bin width to give neutrons/MeV/cm^2. The energies listed in Table IV are the upper bounded for each bin and were chosen, generally, to cover a wide enough energy to give good statistics. The bin boundary at 13.29 MeV was chosen because this represents the low energy point for the direct source neutrons in the 14-MeV peak. These are the neutrons that come out at back angles and scatter into the detector. After averaging, the statistical errors were reduced substantially, and, when combined with the errors associated with background subtraction, were less than 1% in the energy interval 0.3 to 6.0 MeV. In the energy interval below 0.3 MeV and from 6.0 to 13.29 MeV, the largest error from these two sources occurs at 13.29 MeV and is about 10%. In the peak at 14 MeV, the combined statistical error and that associated with background subtraction is about 4%. Over most of the energy range, the largest errors in the experimental results are associated with uncertainty in the detector efficiency. These efficiency-associated errors are 5% in the interval from 2 to 13.29 MeV, 10% in the interval from 1 to 2 MeV, and 15% below 1 MeV. At 14 MeV the detector efficiency introduces no error.

The data obtained with a detector bias of approximately 0.15 MeV were normalized to the data obtained at a bias of approximately 0.85 MeV in the energy region from 1.5 to 5.0 MeV. The composite spectrum obtained from all the data is presented in

TABLE I

RAW DATA OBTAINED WITH TRITIUM IN CELL

Channel Number	Data									
1	0	21	130	8	12	15	15	15	13	12
11	11	16	16	12	12	18	17	8	10	7
21	11	13	9	8	20	17	13	10	7	8
31	12	13	14	11	7	9	18	17	12	18
41	13	17	15	13	8	17	10	14	16	9
51	11	9	13	13	9	9	12	16	17	14
61	11	13	13	9	12	12	15	8	9	19
71	12	14	15	19	15	15	18	11	14	12
81	20	10	13	11	10	11	9	8	13	9
91	17	6	16	10	14	9	15	8	11	7
101	7	8	11	16	11	15	15	17	4	10
111	16	19	15	13	9	10	13	8	13	16
121	16	12	8	9	10	14	12	8	11	13
131	15	12	17	10	16	16	13	17	13	11
141	9	13	11	8	10	15	10	4	11	13
151	8	13	14	10	9	10	11	12	17	17
161	9	13	12	7	16	13	9	9	8	15
171	12	12	11	17	12	16	8	12	12	9
181	14	12	10	18	14	12	10	14	9	12
191	9	13	11	7	11	14	16	16	15	8
201	12	12	10	12	13	6	12	12	16	16
211	6	11	18	17	12	9	16	8	7	18
221	8	9	12	10	11	17	8	14	15	9
231	19	8	14	15	13	16	18	16	12	16
241	3	12	9	12	14	12	10	12	14	20
251	19	9	15	9	11	16	15	16	19	12
261	10	12	18	14	8	18	8	8	10	15
271	9	18	15	17	18	14	15	8	9	13
281	16	23	13	16	10	21	10	10	13	8
291	14	10	10	15	21	12	15	22	12	16
301	11	14	12	18	12	18	12	10	14	13
311	9	11	10	8	18	7	8	15	17	26
321	12	15	12	12	8	18	17	8	18	23
331	9	13	11	17	18	22	29	18	34	48
341	15	13	21	23	40	40	37	35	35	85
351	17	20	27	47	62	67	68	88	88	114
361	27	27	42	62	100	104	111	120	120	180
371	30	58	58	92	149	159	179	187	187	226
381	50	107	92	144	213	213	208	233	233	275
391	100	153	144	187	246	271	285	286	286	354
401	146	227	187	261	331	376	353	384	384	409
411	183	237	261	319	436	412	385	441	441	505
421	272	318	319	393	457	497	479	492	492	539
431	302	381	393	462	542	532	518	549	549	600
441	398	510	462	539	580	561	570	593	593	616
451	469	553	539	624	593	609	639	636	636	627
461	531	559	624	640	624	621	660	640	640	680
471	550	629	640	621	608	659	659	663	663	661
481	624	631	621	619	641	660	657	671	671	609
491	581	633	619	660	666	607	636	568	568	573
501	625	669	660	601	615	615	560	584	584	512
511	650	632	601	576	601	538	558	541	541	426
521	653	619	576	555	442	477	449	444	444	347
531	586	535	555	451	419	376	384	381	381	274
541	536	520	451	398	306	294	318	276	276	195
551	522	422	398	319	204	168	183	186	186	115
561	431	357	319	201	129	129	108	129	129	54
571	331	246	201	127	101	74	62	59	59	26
581	260	159	127	88	50	40	44	25	25	32
591	148	91	88	49	32	28	33	35	35	447
601	99	57	49	33	31	49	56	140	140	11
611	62	31	33	35	49	11	11	5	5	10
621	32	23	35	317	11	15	13	9	9	5
631	30	605	317	18	16	12	17	13	13	9
641	842	10	18	15	17	15	10	11	26	13
651	9	12	15	11	12	9	7	13	41	26
661	6	12	11	13	12	15	17	20	14	41
671	14	10	13	19	12	9	27	30	6	14
681	13	14	18	18	22	15	15	13	7	6
691	19	25	69	10	88	23	19	11	11	7
701	19	62	10	11	7	118	13	15	13	11
711	64	11	11	10	11	9	17	8	12	8
721	12	12	10	11	13	15	13	12	9	9
731	7	11	14	13	15	5	9	9	7	7
741	8	14	9	8	7	12	10	16	16	16
751	6	9	15	11	17	19	13	0	11	11
761	14	15	6	0	11	15	0		0	13
771	11	6	6		0	9				8
781	19	14				0				0
791	12	6								

TABLE II

RAW DATA OBTAINED WITH HELIUM IN CELL

Channel Number	Data									
1	0	12	73	7	4	8	6	5	7	11
11	6	7	9	6	6	6	4	6	6	5
21	7	10	8	5	5	6	9	6	4	6
31	11	9	5	4	10	4	5	11	1	6
41	4	9	6	5	7	4	6	9	9	9
51	5	14	7	5	5	10	9	11	9	4
61	3	11	6	7	9	5	3	9	5	9
71	7	9	8	11	6	13	10	8	2	10
81	7	10	3	3	15	8	3	7	2	5
91	4	13	5	9	3	10	5	8	7	8
101	4	10	6	10	9	6	4	9	10	14
111	8	3	4	5	8	7	8	7	14	3
121	6	10	9	6	10	6	9	5	11	5
131	14	12	6	4	5	10	11	8	12	6
141	5	6	5	8	7	6	11	3	4	15
151	4	10	5	5	7	7	8	13	7	10
161	5	8	5	6	3	10	6	4	3	4
171	10	1	15	8	11	10	10	5	8	10
181	6	9	3	9	4	4	6	7	4	3
191	4	13	4	11	14	5	11	2	7	9
201	6	6	7	3	4	10	14	6	9	5
211	6	6	6	7	12	7	11	3	7	7
221	5	6	7	5	7	7	5	10	6	2
231	6	3	7	9	10	4	6	5	7	3
241	10	3	8	10	3	9	9	6	7	10
251	4	14	8	6	2	13	4	8	9	6
261	8	6	4	7	6	7	9	9	9	7
271	12	13	10	7	10	10	9	3	7	12
281	9	5	8	6	4	12	10	4	10	9
291	10	3	5	9	5	11	9	1	5	6
301	4	5	8	7	4	4	4	7	7	3
311	3	8	11	4	8	4	10	8	10	9
321	7	9	8	5	7	6	8	10	5	4
331	4	9	5	5	4	3	6	7	4	5
341	6	6	10	7	8	9	5	5	5	9
351	8	8	9	4	6	9	9	11	6	7
361	7	8	8	7	6	10	8	10	10	15
371	6	10	4	5	4	8	7	7	6	10
381	12	13	8	9	9	4	9	7	6	7
391	17	7	6	14	9	5	9	5	11	8
401	14	7	8	13	18	7	8	6	13	9
411	11	19	13	16	13	12	10	14	12	18
421	9	13	12	7	15	15	15	16	15	16
431	19	17	15	16	14	18	17	11	23	14
441	14	22	18	21	21	23	20	25	20	24
451	15	18	20	14	17	23	13	21	29	26
461	22	23	21	24	20	23	21	25	23	33
471	27	38	29	25	23	32	17	34	31	36
481	38	25	29	21	28	27	24	31	23	16
491	17	11	15	15	24	14	10	26	18	13
501	18	20	16	14	22	14	22	21	16	19
511	26	21	18	23	21	20	27	32	24	18
521	16	21	14	17	16	20	16	13	15	17
531	13	20	11	13	13	16	17	15	11	16
541	13	12	15	15	12	20	20	18	14	24
551	19	13	20	14	17	14	12	15	6	20
561	16	10	14	23	16	22	16	21	21	29
571	22	24	31	22	27	21	16	6	9	9
581	5	7	8	9	5	5	22	11	5	10
591	10	7	8	13	7	11	10	10	7	6
601	7	7	9	7	7	10	3	5	13	6
611	7	7	7	7	8	10	6	5	7	9
621	2	9	11	6	11	8	5	4	9	6
631	10	13	7	9	9	7	9	8	11	18
641	5	10	8	5	7	4	5	4	4	4
651	8	8	4	8	6	8	8	7	12	6
661	4	4	10	5	6	8	5	4	11	4
671	7	11	5	7	10	9	8	5	10	2
681	7	7	8	6	7	7	5	7	7	7
691	9	4	7	6	9	4	6	5	7	2
701	6	9	9	6	12	6	3	9	12	2
711	6	4	8	6	10	10	7	6	7	5
721	6	10	6	8	5	6	4	5	8	5
731	8	5	10	10	9	8	8	5	3	7
741	7	6	5	5	8	6	6	3	4	10
751	15	7	7	8	5	9	6	7	6	4
761	11	9	8	5	8	6	6	5	5	5
771	5	6	8	5	6	12	6	4	7	7
781	8	6	8	6	11	6	10	4	6	4
791	1	2	0	0	0	0	0	0	0	0

TABLE III

REDUCED DATA FROM TABLES I AND II

CHANNEL NUMBER	ENERGY	DATA	NEUT/MEV	ERROR
435	1.402	353.8	1.668E-08	9.207E-10
440	1.450	349.8	1.456E-08	8.149E-10
445	1.502	387.9	1.454E-08	7.822E-10
450	1.555	409.0	1.387E-08	7.293E-10
455	1.612	477.4	1.470E-08	7.002E-10
460	1.672	470.3	1.320E-08	6.449E-10
465	1.736	509.5	1.308E-08	6.045E-10
470	1.803	502.4	1.182E-08	5.635E-10
475	1.874	535.7	1.157E-08	5.234E-10
480	1.949	571.8	1.137E-08	5.067E-10
485	2.029	578.9	1.061E-08	4.639E-10
490	2.114	579.9	9.818E-09	4.206E-10
495	2.204	595.0	9.314E-09	3.986E-10
500	2.301	645.3	9.352E-09	3.770E-10
505	2.404	635.2	8.532E-09	3.514E-10
510	2.514	616.1	7.676E-09	3.200E-10
515	2.631	637.2	7.370E-09	3.026E-10
520	2.757	615.1	6.609E-09	2.753E-10
525	2.893	589.0	5.882E-09	2.499E-10
530	3.038	595.0	5.526E-09	2.339E-10
535	3.195	600.0	5.185E-09	2.171E-10
540	3.365	544.7	4.380E-09	1.940E-10
545	3.548	523.6	3.920E-09	1.760E-10
550	3.747	469.3	3.271E-09	1.593E-10
555	3.963	457.3	2.968E-09	1.446E-10
560	4.198	399.0	2.411E-09	1.274E-10
565	4.455	356.8	2.008E-09	1.117E-10
570	4.737	323.6	1.696E-09	1.032E-10
575	5.046	263.3	1.286E-09	8.773E-11
580	5.386	229.2	1.042E-09	7.224E-11
585	5.762	158.8	6.726E-10	5.585E-11
590	6.179	160.8	6.341E-10	5.378E-11
595	6.643	117.6	4.318E-10	4.293E-11
600	7.162	86.5	2.955E-10	3.478E-11
605	7.744	62.3	1.983E-10	2.871E-11
610	8.400	45.2	1.340E-10	2.338E-11
615	9.144	27.1	7.481E-11	1.915E-11
620	9.992	12.1	3.046E-11	1.499E-11
625	10.965	12.1	2.761E-11	1.435E-11
630	12.087	13.1	2.713E-11	1.139E-11

TABLE IV

MEASURED NEUTRON SPECTRUM FROM ORALLOY SPHERE

E_n [a] (MeV)	Neutrons/MeV-cm^2/Source Neutron at the Detector x 10^{-9}	Error (%)
16.0	0.98	4
13.29	0.042	15
10.0	0.089	12
8.0	0.358	8
6.0	1.60	6
4.0	4.21	5
3.0	6.99	5
2.5	9.6	5
2.0	11.8	10
1.8	13.3	10
1.6	15.3	10
1.4	17.1	10
1.2	19.9	10
1.0	21.1	15
0.9	23.4	15
0.8	25.4	15
0.7	28.5	15
0.6	31.6	15
0.5	32.6	15
0.4	31.1	16
0.3	29.4	20
0.2	23.6	25
0.18	---	---

[a] Upper boundary of energy bin.

Table IV, along with the total experimental uncertainty for each energy bin. This uncertainty was obtained by simply adding the statistical uncertainty in each energy bin to the uncertainty from the detector efficiency.

IX. COMPARISON WITH MONTE CARLO CALCULATIONS

Monte Carlo calculations were performed by LASL's Theoretical Design Division with the code MCN.[10] The detailed geometry shown in Fig. 12 was used in these calculations with a point detector positioned at 0° to the beam at a distance of 38.87 m from the source. The effect of the collimating system and concrete walls was simulated by setting the cell importance to zero for those cells outside the volume defined by a 30.5-cm-diam cylinder from the source to the detector. When a neutron was scattered into this volume outside the cylinder, its weight was set to zero and its path was no longer followed.

The measured energy and yield as a function of angle (Fig. 6) were used in the source subroutine for these calculations. The sphere geometry used in the code is shown in Fig. 7. Neutrons per square centimeter were tallied in the energy bins of Table IV and then divided by the energy bin width to give neutrons/MeV-cm^2/source neutron. Statistical errors of 2% or less were acquired in several hours of computer time for most energy bins, with the largest error of approximately 5% occurring for the 10- to 13.29-MeV bin.

Cross-section sets from LLL and ENDF/B-IV were used to calculate the spectrum. These calculated results are presented in Table V. Figure 15 shows a comparison of the experimental results with the calculated results using the two cross-section sets. The experimental results are plotted at the midpoint of each energy bin and the calculated results are shown as curves from the midpoint of one bin to the next. Both sets of results are in reasonable agreement with the experimental results. However, the ENDF/B-IV cross-section set does provide much better agreement, and in the region from 1 to 6 MeV the agreement is excellent. Both cross-section sets appear to predict a harder spectrum above 6 MeV than is observed, and the worst agreement is in the 10- to 13.29-MeV bin where the statistical errors, both for experimental and calculational results, are the largest. Future experiments are planned to cover more fully the region below a few hundred keV.

REFERENCES

1. R. E. Hunter, Los Alamos Scientific Laboratory, private communication, March 4, 1974.

2. C. E. Ragan, Los Alamos Scientific Laboratory, private communication, Sept. 27, 1974.

3. Leona Stewart and Gerald M. Hale, "The T(d,n)^{4}He and T(t,2n) Cross Sections at Low Energies," Los Alamos Scientific Laboratory report LA-5828-MS (Jan. 1975).

4. John D. Seagrave, "D(d,n)HE^3 and T(d,n)He^4 Neutron Source Handbook," Los Alamos Scientific Laboratory report LAMS-2162 (Nov. 1957).

TABLE V

CALCULATED NEUTRON SPECTRUM FROM ORALLOY SPHERE

E_n [a] (MeV)	Neutron/MeV-cm^2/Source Neutron x 10^{-9} LLL Cross Sections	Neutron/MeV-cm^2/Source Neutron x 10^{-9} ENDF/B-IV Cross Sections
16.0	0.86	0.94
13.29	0.044	0.044
10.0	0.125	0.140
8.0	0.41	0.48
6.0	1.55	1.58
4.0	3.7	4.1
3.0	5.8	6.5
2.5	7.8	9.1
2.0	9.6	11.3
1.8	11.0	13.5
1.6	13.0	15.0
1.4	15.0	16.5
1.2	18.0	20.0
1.0	21.5	21.5
0.9	22.5	23.5
0.8	25.0	25.5
0.7	28.0	27.0
0.6	31.5	29.5
0.5	34.0	30.5
0.4	34.5	31.0
0.3	31.5	27.5
0.2		

[a]Upper boundary of energy bin.

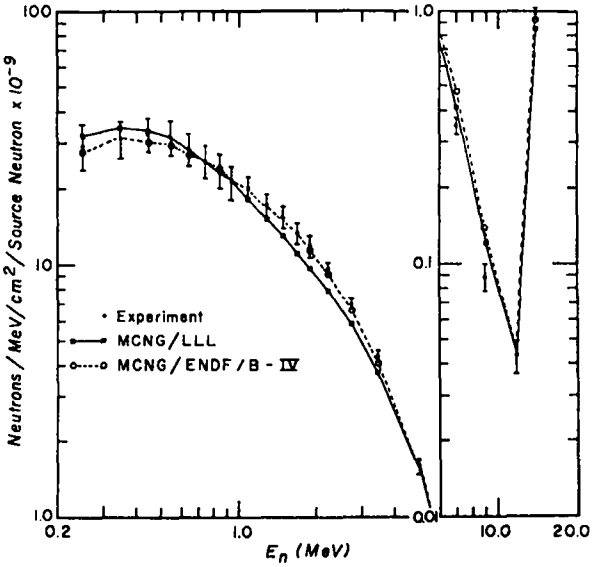

Fig. 15.
Comparison of the experimental and calculated spectrum from the 38-kg oralloy sphere at the detector in neutrons/cm^2/MeV/source neutron. The Monte Carlo code MCN was used to obtain the calculated results, and in these calculations two sets of cross sections were used—one from LLL and one from the ENDF/B-IV library. The results from the ENDF/B-IV calculation are in excellent agreement with the experiment and are a substantial improvement over the calculations using the LLL cross sections, especially in the 1- to 6-MeV energy region.

5. H. V. Argo, R. F. Taschek, H. M. Agnew, A. Hemmendinger, and W. T. Leland, "Cross Sections of the D(T,n)He^4 Reaction for 80- to 1200-keV Tritons," Phys. Rev. 87, 612 (1952).

6. See, for example, I. J. Taylor and J. Kalyna, "A High Speed Pulse Shape Discriminator," Nucl. Instrum. Methods 88, 267 (1970).

7. V. V. Verbinski, W. R. Burrus, T. A. Love, W. Zobel, N. W. Hill, and R. Textor, "Calibration of an Organic Scintillator for Neutron Spectrometry," Nucl. Instrum. Methods 65, 8 (1968).

8. H. Liskien and A. Paulsen, "Neutron Production Cross Sections and Energies for the Reactions T(p,n)^{3}He, D(d,n)^{3}He, and T(d,n)^{4}He," Nucl. Data Tables 11, 569 (1973).

9. M. Drosg and D. M. Drake, "Absolute Differential Cross Sections for Neutron Production by the ^{2}H(d,n)^{3}He Reaction with E_d from 6 to 17 MeV and by the ^{3}H(p,n)^{3}He Reaction with E_p from 6 to 16 MeV," Los Alamos Scientific Laboratory report LA-5732-MS (Dec. 1974).

10. E. D. Cashwell, J. R. Neergaard, W. M. Taylor, and G. D. Turner, "MCN: A Neutron Monte Carlo Code," Los Alamos Scientific Laboratory report LA-4751 (Jan. 1972); E. D. Cashwell, J. R. Neergaard, C. J. Everett, R. G. Schrandt, W. M. Taylor, and G. D. Turner, "Monte Carlo Photon Codes: MCG and MCP," Los Alamos Scientific Laboratory report LA-5157-MS (1972); R. G. Schrandt, "MCNG - Running Instructions," Los Alamos Scientific Laboratory, private communication (1973).